Journal of Polymer Research (2022) 29: 318
https://doi.org/10.1007/s10965-022-03180-6

ORIGINAL PAPER

# Mechanical performances, in-vitro antibacterial study and bone stress prediction of ceramic particulates filled polyether ether ketone nanocomposites for medical applications

**Aezhisai Vallavi Muthusamy Subramanian**[1] · **Mugilan Thanigachalam**[1]

Received: 18 January 2022 / Accepted: 4 July 2022 / Published online: 11 July 2022


**Abstract**
Polyether ether ketone (PEEK) and PEEK composites are viable candidates for dental and ortho implants due to their superior properties. This research aims to develop the functionalized ceramic nanoparticles such as $TiO_2$ (T-NPs) and $SiO_2$ (S-NPs) reinforced biopolymer nanocomposites by injection moulding. The morphologies of fabricated composite group were analysed by FE-SEM. The effect of T-NPs, S-NPs, and combined effect of TS-NPs of different wt.% reinforcements (4, 8, 12, 16, and 20 wt.%) with PEEK matrix on mechanical properties such as tensile, flexural, compressive, and shore D hardness had been investigated. The excellent mechanical strengths were obtained in 16 wt.% T/PEEK, 12 wt.% S/PEEK, and 16 wt.% TS/PEEK group. Then, the in-vitro antibacterial property of these selected composite group was investigated and found improved antibacterial activity compared to neat PEEK. Four different thread profiles were selected and analysed using 3D-FEM to reduce the stress distribution at bone-implant contact region. The minimum stress distribution range was achieved in the cortical bone model as 0.11–1.74 MPa due to trapezium profile threaded implants. Thus, the developed composites were found to be promising material for medical implant applications.

**Keywords** Biomaterials · Polymer nanocomposite · Mechanical properties · Dental implant · Bone stress · FESEM

## Introduction

Dispersion of nanoparticles can modify the mechanical properties of polymer nanocomposites. Interfacial interaction between the organic and inorganic phases impacts the different properties of the polymer nanocomposites [1]. However, the change in properties of the polymer nanocomposites depends on the amount, shape, and size of the particles and matrix interaction with nano fillers [2]. These interface interactions of nano and micro-sized fillers with different weight percentage resulted in enhanced mechanical properties [3].

Dental polymeric materials such as PEEK, PMMA, and PLA were recently researching alone with various reinforcement by melt blending compounding using a twin-screw extruder. The traditional hardness, Marten's hardness, and scratch hardness were greater for composites than pure PMMA. The mechanical properties are improved due to the addition of $TiO_2$ with the polymer matrix [4]. The result of $TiO_2$ on photo and biodegradation of PLA/LDPE blend films was investigated. The tensile strength, modulus, and elongation were decreased after photodegradation for four weeks at the breaking point [5, 6]. The HDPE/$TiO_2$ nanocomposites with varying nanofillers were prepared using injection moulding. An increase in the concentration of $TiO_2$ in the HDPE matrix improves the stiffness of the nanoparticle by 10%, which leads to higher wear resistance [7].

The $SiO_2$ nanospheres (SNS/UHMWPE) filled nanocomposites were prepared by solgel method. Adding $SiO_2$ increases the tensile modulus of the pristine UHMWPE, but SNS fillings decrease the tensile modulus and elongation at break, which shows low toughness. Since the pure UHMWPE have lower young's modulus and yield strength and excellent elongation at break. The properties of the produced UHMWPE show stable tensile modulus, yield strength, and elongation at break [8]. Significant improvements in the mechanical properties were observed in the polymer

✉ Mugilan Thanigachalam
mugilangct@gmail.com

[1] Department of Mechanical Engineering, Government College of Technology, Coimbatore 614 013, Tamil Nadu, India

nanocomposites by adding S-NPs. Micro-sized filler shows less influence in Modulus elasticity, which can be increased by increasing fillers size to nano scale. The surface treatment of S-NPs increases the modulus of elasticity, whereas the toughness and stiffness of the polymer nanocomposites depend on the interfacial interaction [9]. The inclusion of S-NPs in the polymer matrix shows higher fracture toughness under the deformation of the polymer nanocomposites [10, 11]. To achieve high-performance polymer nanocomposites, spatial distribution and structural property relationships must be accurate [12].

The important deciding factors influencing the successful biomedical implantation were stresses and forces transferred to the interface between bone and implant region. These kinds of stresses and actions of forces decide the primary implant stability [13]. Normally periodontal ligament absorbs the stress distribution and gives the cushioning effort elements to the occlusal forces due to the tooth structure. The dental implants can fail due to several factors such as stress transition around the bone thread profile shape and profile, the pitch of thread, face angle, and helix angle of the thread. Also, the effect of stress distribution directly influences the implant success rate [14].

The optimal values of the selected factors on parameter analysis are essential for proper implant alignment in biomedical applications. The implant selection for further clinical research was based on material and mechanical analysis of the implant design [15]. The Finite Element Method (FEM) and elasticity test give the sensitivity analysis report of the stress distribution of implantation regime and implant structure. From the bone and implant stress analysis through FEM, the optimal length and thread pitch of the implant were found to be 13 mm and 0.7 mm, respectively [16]. Evaluation of successive osseointegration is crucial to the implantation. After implantation, the bonding between the bone and implant was disturbed by several mechanical factors. A primary factor is stress distribution while osseointegration and geometrical features implant. Under buccolingual loading conditions, the effect of different thread-profiled implants on stress distribution was analyzed using FEM [17]. The cortical and cancellous bone experiences stress during implant integration to replace the missed or damaged tooth. The initial analysis was carried out as a non-working movement of the mandibular bone structure. Long term performance of implantation was analyzed previously with clinic researches [18, 19]. These kinds of clinical researches want mechanical analysis about the functionality of the material with occlusion load and some limiting support load for the bone structure presented around the implants [20]. The materialistic characterization such as FTIR, XRD, DSC and TGA for T-NPs and S-NPs reinforced PEEK polymers and only the biocompatible assessments through various in-vitro investigations have been studied in the previous work. The presence of important functional groups such as C = O, T-O-T, Si–O-Si, -OH and C-H have been confirmed. The excellent thermal stability also observed due to the addition of T-NPs and S-NPs ceramic reinforcements. The critical peaks also been identified to for the confirmation of T-NPs and S-NPs addition in to the PEEK matrix [21, 22]. This present work extensively investigates the mechanical performances of PEEK based composites.

### Present work

In this research, the functionalized ceramic particulates reinforced PEEK polymer nanocomposites had been developed and investigated for biomedical applications. The functionalized ceramic particles such as T-NPs and S-NPs were used as reinforcement to fabricate the composites through the injection moulding process. FESEM (Field Emission Scanning Electron Microscopy) investigated the structural morphology of developed polymer nanocomposites. The element presence was confirmed with the help of EDAX (Energy Dispersive X-Ray) elemental analysis. The mechanical properties such as tensile, compressive, flexural, shore D hardness were investigated as per the ASTM standards. Best wt.% was chosen in each group based on compressive strength and hardness values. In-vitro antibacterial activity against *E. coli* and *B. subtilis* in the absence of UV–Vis irradiation was adopted to evaluate the antibacterial property for those chosen groups. Mechanical properties of those selected groups were used as input parameters for 3D FEM (Finite Element Method) to predict the bone stress by different thread profiled (trapezium, buttress, reverse buttress, and square) dental implant model.

## Experimental methodology

### Materials

PEEK pellets (Medical Grade) purchased from Engineered Polymers Ind. Pt Ltd., Mumbai, India, whose melting point is 343 °C, had been employed as a matrix material. From Sisco Research Laboratory in Mumbai and AD Nano Technologies Pvt Ltd in Karnataka, the ceramic T-NPs and S-NPs were purchased, respectively. T-NPs and S-NPs had melting points of 1843 °C and 1710 °C, respectively. The molecular weight of PEEK is 328.3 g/mol. Using particle size analyzer, the average particle sizes of T-NPs and S-NPs were measured as 21.56 nm and 7.53 nm, respectively. The molecular weight of PEEK polymer is 328.3 g/mol.

## Synthesis of functionalized NPs

The purchased ceramic T-NPs and S-NPs were introduced into the functionalization process of acrylic acid in order to enhance the biocompatible activities of medical implant materials. Each of the T-NPs and S-NPs was combined with 30 g of acrylic acid. The 32 g of hexane solution was diluted in water to introduce the new combination. It took around 20–30 min to sonicate the prepared mixer. Then the mixture was allowed to cool to ambient temperature. In order to remove the adsorbed residues from the mixture, it was centrifuged for up to two hours at 13,000 rpm. It was then dried in a vacuum chamber to produce functionalized nanoparticles [23, 24].

## Fabrication of polymer nanocomposite

A vertical plastic injection moulding procedure was used to develop the functionalized ceramic T-NPs and S-NPs reinforced PEEK polymer nanocomposite. The different wt.% of reinforcements with the PEEK matrix as shown in Table 1. T-NPs and S-NPs were preheated before being combined with the PEEK polymer and fed into the moulding machine in the correct ratios. The heating chamber was kept at a temperature between 100 and 120 °C in order to blend the NPs with the semi-solid PEEK polymer. The structure of the both functionalized T-NPs and S-NPs are rutile tetragonal structure. Due to the blend mixing method the T-NPs and S-NPs are bonded with the PEEK matrix. Using a vertical injection moulding machine, 45–50 bar of pressure was maintained to inject the PEEK matrix and ceramic reinforcement into the die cavity. After that, the die was opened, and the composite specimens that had been moulded were removed [25, 26].

## FESEM morphological characterization with EDAX analysis

Fabricated functional ceramic T-NPs and S-NPs reinforced polymer nanocomposite specimens' surface morphologies were studied with the help of FESEM. The EDAX analysis was adopted to detect and confirm the elements presence and composition in the fabricated polymer nanocomposite specimens.

## Mechanical characterization

The influence of functionalized nanoparticles in PEEK were tested on mechanical properties such as tensile, compressive, flexural, and shore D hardness tests. Mean values for each combination were calculated from three samples to allow statistical analysis. A universal testing machine was used to conduct the tensile tests. Each testing sample was fabricated according to ASTM standards as shown in Fig. 1. The ASTM standards for preparing tensile, flexural, shore D hardness, and compressive testing were ASTM-D638, ASTM-D790, ASTM-D2240, and ASTM-D695, respectively. Before the 3-point bending test, the specimen dimensions were measured by a digital compass of 0.01 sensitivity. Measurements were performed at 3 points for the width and height, and their average values were used in the calculation of bending strength. The 3-point bend test was performed according to the ASTM-D790 and specifications in such a way that the diameter for both supports was 2 mm and the span in between supports was 20 mm [27]. During the test, the cross head speed was adjusted as 0.1 mm/min. Maximum load was recorded before the fracture. In this study, the force–deflection curves were obtained. The flexural stress, flexural strain, and flexural modulus were computed using the following Eqs. (1), (2), and (3), respectively.

**Table 1** Different wt.% of fabricated composite samples with codes

| Group and wt.% | Actual composition of reinforcement and matrix | | | Sample codes | | |
|---|---|---|---|---|---|---|
| | T/PEEK | S/PEEK | TS/PEEK | T/PEEK | S/PEEK | TS/PEEK |
| **4 wt.%** | 4 wt.% $TiO_2$ + 96 wt.% PEEK | 4 wt.% $SiO_2$ + 96 wt.% PEEK | 2 wt.% $TiO_2$ + 2 wt.% $SiO_2$ + 96 wt.% PEEK | 4% T/PEEK | 4% S/PEEK | 4% TS/PEEK |
| **8 wt.%** | 8 wt.% $TiO_2$ + 92 wt.% PEEK | 8 wt.% $SiO_2$ + 92 wt.% PEEK | 4 wt.% $TiO_2$ + 4 wt.% $SiO_2$ + + 92 wt.% PEEK | 8% T/PEEK | 8% S/PEEK | 8% TS/PEEK |
| **12 wt.%** | 12 wt.% $TiO_2$ + 88 wt.% PEEK | 12 wt.% $SiO_2$ + 88 wt.% PEEK | 6 wt.% $TiO_2$ + 6 wt.% $SiO_2$ + + 88 wt.% PEEK | 12% T/PEEK | 12% S/PEEK | 12% TS/PEEK |
| **16 wt.%** | 16 wt.% $TiO_2$ + 84 wt.% PEEK | 16 wt.% $SiO_2$ + 84 wt.% PEEK | 8 wt.% $TiO_2$ + 8 wt.% $SiO_2$ + + 84 wt.% PEEK | 16% T/PEEK | 16% S/PEEK | 16% TS/PEEK |
| **20 wt.%** | 20 wt.% $TiO_2$ + 80 wt.% PEEK | 20 wt.% $SiO_2$ + 80 wt.% PEEK | 10 wt.% $TiO_2$ + 10 wt.% $SiO_2$ + 80 wt.% PEEK | 20% T/PEEK | 20% S/PEEK | 20% TS/PEEK |

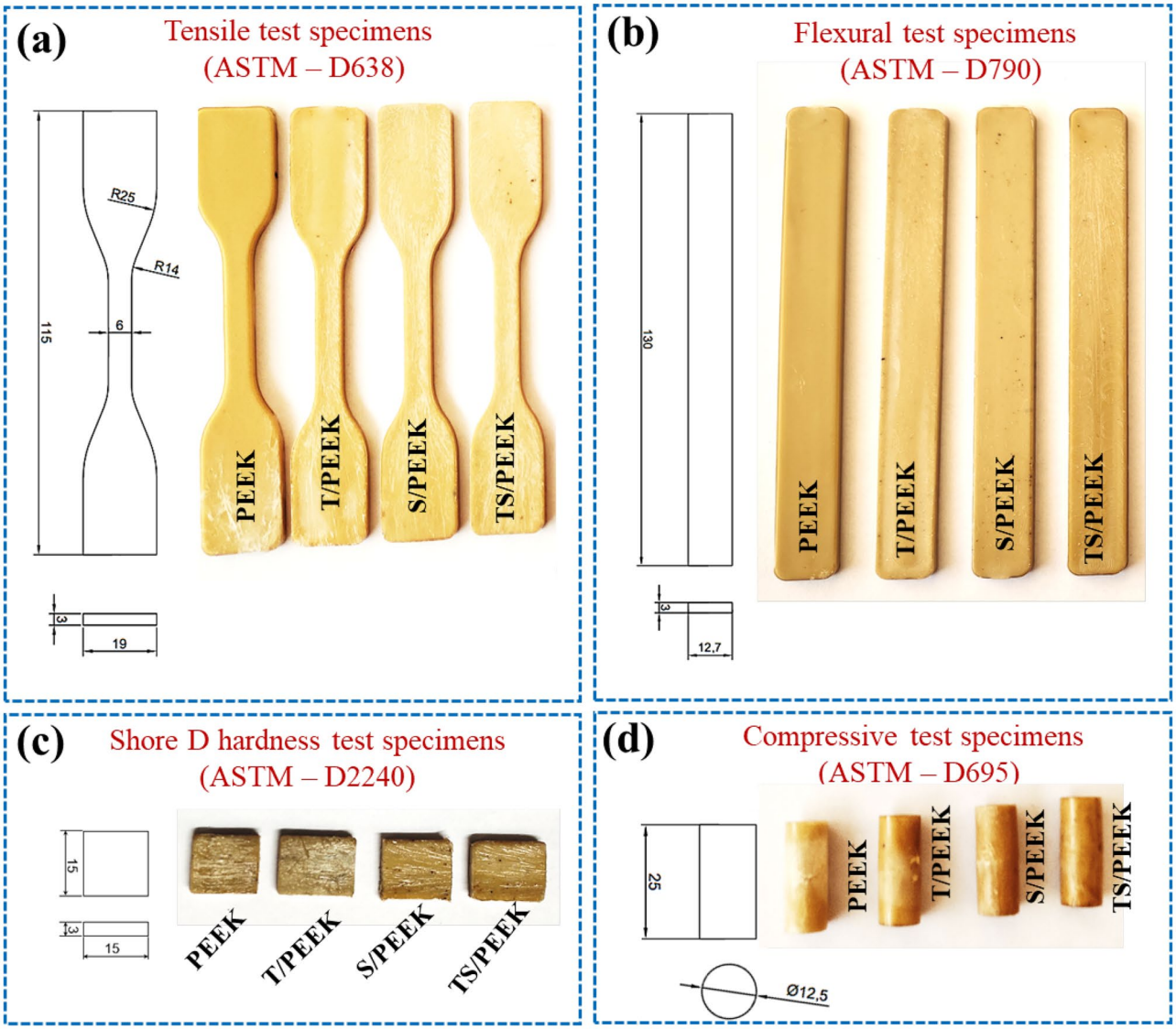


**Fig. 1** Fabricated composite samples according ASTM standards

$$\sigma_f = \frac{3Fl}{2bd^2} \tag{1}$$

$$\varepsilon_f = \frac{6\delta d}{l^2} \tag{2}$$

$$E_f = \frac{\sigma_{f2} - \sigma_{f1}}{\varepsilon_{f2} - \varepsilon_{f1}} \tag{3}$$

where $\sigma_f$ is the flexural strength (in MPa), $F$ is the maximum load applied to the specimen (N), $\delta$ is the deflection and $l$ is the span in between the supports (20 mm), and $b$ and $h$ are width and thickness of specimen in mm, respectively.

## Bone stress prediction using 3D FEM

### Bone and implant materials

The four-thread profile was designed: Trapezium, buttress, reverse buttress, and square. The implant material was assigned as polymeric ceramic composite properties: T/PEEK, S/PEEK, and TS/PEEK groups. The material for two types of bone is cortical and cancellous. The cortical bone material and cancellous bone material are assigned to the respective CAD models. The young's modulus, poisson's ratio and density for cortical and cancellous bone [28, 29] are listed in Table 2.

**Table 2** Bone material properties

| Material | Young's modulus (MPa) | Poisson ratio | Density ($g/cm^3$) |
|---|---|---|---|
| **Cortical bone** | 13,700 | 0.3 | 1.6 |
| **Cancellous bone** | 1370 | 0.3 | 0.3 |

### Modeling and 3D finite element method

The IGES format is used for importing the CAD files to the FEM analysis purpose using ANSYS 18. Discretization or subdivision of the model into number of finite elements. These elements are met at various intersections, which are called nodes. The following procedures had been adopted for model development and FEM analysis. 3D FEM model for bone structure geometries was created to predict the distribution of bone stress around the implants caused by the application of inclined load called buccolingual load. The bone structure is an isotropic, homogenous, linearly elastic material of constants like young's modulus and Poisson ratio listed in Table 2. In all directions, the properties of the isotropic model remain the same. The simulation started from outer layer of bone structure, which is cortical bone, and then cancellous bone where the implant was placed. The whole implant body is embedded with bone structure.

The shape of the various profile is shown in Fig. 2. It clearly shows the dimensions of the implant body, which has 13 mm length, 4 mm diameter, 1.2 mm thread pitch and 0.45 mm thread depth, and 30° thread angulation. Cortical bone is subjected to fixed support in this simulation's boundary condition. This osseointegration is perfect, which means that the bond between the bone structure and implant body is perfect throughout the entire interference.

The number of nodes and elements identified after meshing in trapezium, buttress, reverse buttress, and square shape profile thread is 13716, 14,813, 13,735, 12,837, and 71,459, 73,708, 70,975, respectively. The meshed models were subjected to analysis was showed in Fig. 3. Loading condition is necessary while analyzing the static structural analysis. The buccolingual load of 60 N has been assigned for each material implant. The density of the Mesh model plays an

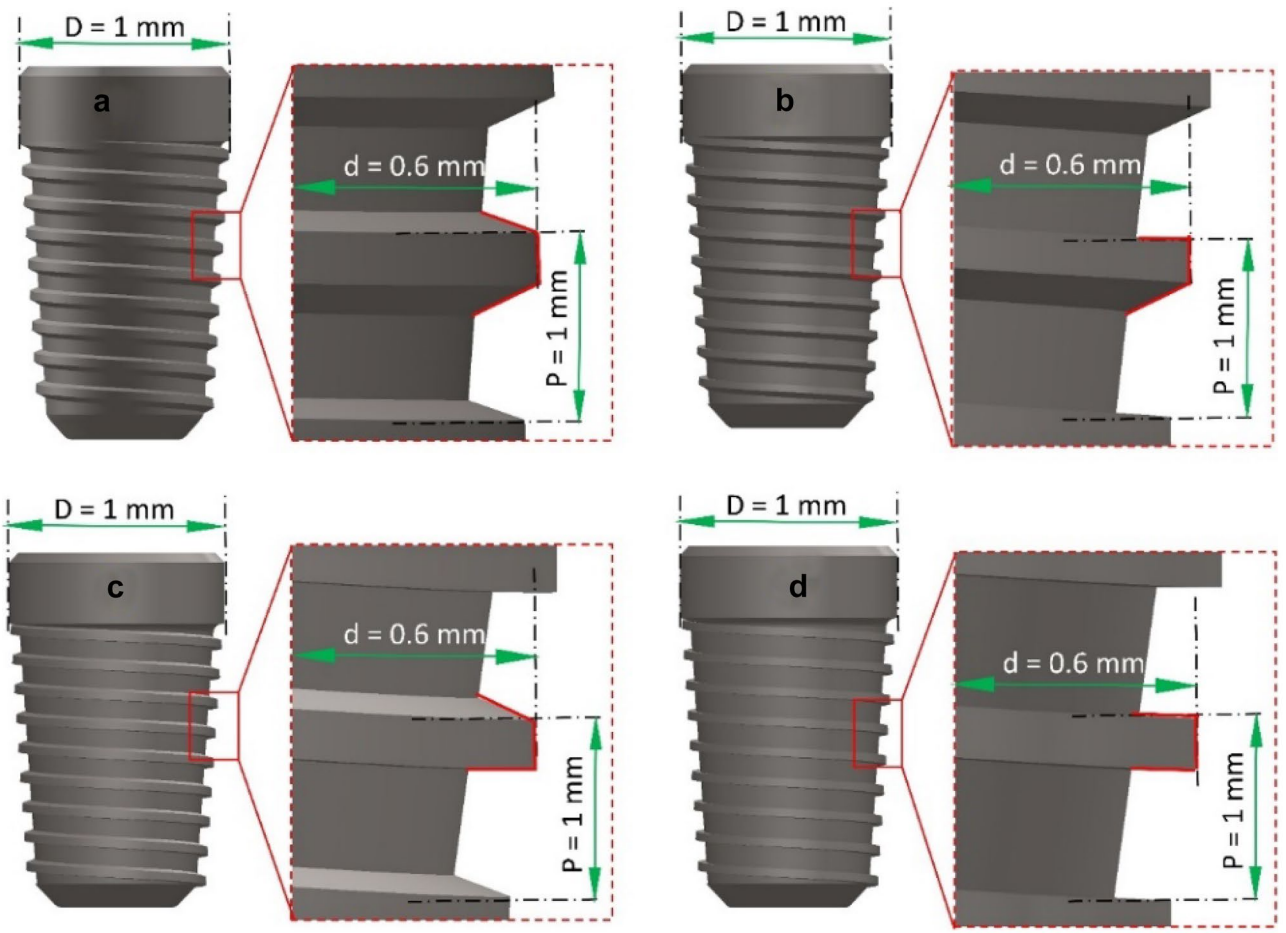


**Fig. 2** Various thread profiled implant design **a** Trapezium, **b** Buttress, **c** Reverse buttress, **d** square

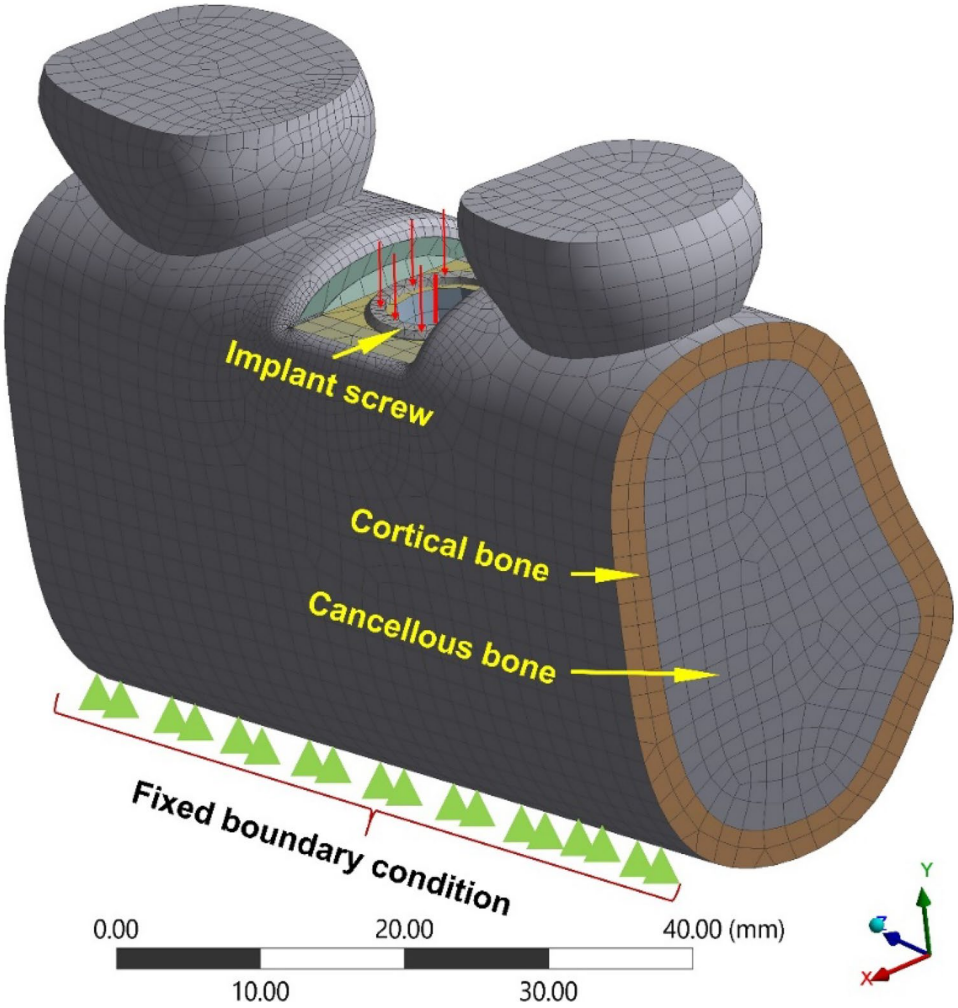


**Fig. 3** Meshed view of human bone system and implant model

essential role in increasing the accuracy of the results in all the stress regions. The required minimum number of elements is 25000–200,000, and the minimum number of nodes must be 140–300 µm. The meshed model used in this analysis implied various assumptions related to simulation geometries.

## In-vitro antibacterial assessment

The in-vitro antibacterial activity of PEEK and polymer composite groups was investigated against two prokaryotic strains. The samples were analyzed qualitatively using disc diffusion. The antimicrobial microorganisms employed were *Escherichia coli* (*E. coli*, model gram-negative bacteria) and *Bacillus subtilis* (*B. subtilis*, model gram-positive bacteria) [30, 31]. *E. coli* and *B. subtilis* inoculums were cultured from overnight Luria Broth cultures and incubated at 37 °C for 24 h. It was done by overlaying nutritious agar in 4 mm thick petri plates. They were inoculated into semi-confluent growth as 2 µl dense inoculums of E. coli and B. subtilis test organisms. Then they were dried in the air for 10 min. The PEEK and PTS composite samples were incubated at 37 °C for 24 h [32]. After incubation, the antibacterial activity of the PEEK and polymer composite group samples was identified by measuring the zone of inhibition (mm).

## Statistical analysis

The mean and standard deviation were calculated for each trial with four repetitive measurements, and the results were compared. For the t-test, Minitab 19 (one-way ANOVA) was used to evaluate the statistical data. A significance level of P is $< 0.05$ was considered to be appropriate.

## Results and discussions

### FE-SEM morphological characterization with EDAX analysis

The structural morphology of fabricated ceramic particulates filled polymer nanocomposites was investigated under FE-SEM analysis. The FE-SEM morphologies of neat PEEK sample, T/PEEK, S/PEEK, and TS/PEEK group composites

are shown in Fig. 4a-d. The proper distribution of T-NPs and S-NPs into the PEEK matrix was observed from those morphological images. The solid bonding between the NPs and PEEK matrix was observed from the FE-SEM analysis. These phenomena were monitored in the composite samples due to the addition of functionalized NPs. The functionalization of NPs provided excellent bonding characteristics between the matrix and reinforcements [33]. Proper dispersion of NPs with PEEK during the injection moulding process was confirmed with the help of the FE-SEM morphologies of developed polymer nanocomposite samples. In a few regions, the agglomerations of NPs with the PEEK matrix were also identified [34]. This can lead to the fracture initiation of the composites and cause tensile fractures [35].

Based on the FESEM observations, the less agglomerations are identified in the all combinations of reinforced polymer composites. This phenomenon pronouns the benefits of nanoparticles and interface with the matrix materials, which is a strong reinforcement in polymer nano composites. The neat PEEK sample, T/PEEK, S/PEEK, and TS/PEEK group composites were characterized by EDAX spectral analysis shown in Fig. 4e–f, which confirmed the presence of elements in the fabricated composites. Also identified the weight percentages and atomic percentages of composite samples. With the help of C and O elements, presence in the EDAX spectrum confirmed the PEEK material with weight percentages of 69.37% and 30.73%, respectively. The T-NPs were confirmed in the T/PEEK group with the help of 10.27 wt.% of Ti elements and atomic % of 2.92. The presence of S-NPs in the S/PEEK group composite was confirmed with Si elements of 12.14 wt.% and 5.89 atomic %. In the TS/PEEK group, the wt.% of Ti and Si elements were confirmed as 6.31 and 5.9, respectively. The atomic wt.% of Ti and Si elements in TS/PEEK was observed as 3.18 and 1.79, respectively.

## Tensile properties of TS/PEEK composites

The effect of functionalized reinforcements such as T-NPs and S-NPs towards tensile, elongation, and young's modulus has been investigated by the universal tensile testing machine according to ASTM-D638. The tensile test result for pure was shown in Fig. 5a. The stress–strain curves for different wt. % T-NPs, S-NPs, and combined TS-NPs reinforced polymer nanocomposites were shown in Fig. 6a-c. Figure 6d clearly showed that increasing the wt.% of T-NPs reinforcement with the PEEK matrix increased tensile strength. This is because functionalized T-NPs were fully bonded with the PEEK matrix [36, 37], and the tensile strength range was observed as 87.761 to 97.945 MPa. The addition of S-NPs revealed that decreases in tensile strength. And maximum and minimum tensile strength of S-NPs/PEEK composites were observed as 102.651 MPa and 91.432 MPa, respectively. The combined addition of TS-NPs decreases tensile properties up to 16% of TS-NPs of fabricated nanocomposites. After that, it tends to increase with the addition of TS-NPs on the PEEK matrix. The maximum and minimum tensile strength was 106.747 MPa and 91.659 MPa, respectively.

The elastic modulus of PEEK, T/PEEK, S/PEEK, and TS/PEEK composite materials were shown in Fig. 6e. The addition of T-NPs into PEEK provided increased elastic modulus, and the range of elastic modulus was found as 3.913 GPa to 6.745 GPa. The addition of S-NPs and TS-NPs into PEEK gives the high elastic modulus properties up to 16 wt.% reinforcement. A further addition to reinforcement, the elastic modulus value gets decreases. The highest elastic modulus was observed in T/PEEK, S/PEEK, and TS/PEEK were 5.757 MPa at 16 wt.% of T-NPs, 5.563 MPa at 12 wt.% of S-NPs, and 6.745 MPa at 16 wt.% of TS-NPs respectively. Addition of ceramic reinforcement into to PEEK matrix enhanced the elastic modulus property, which reached near the young's modulus of human cortical and cancellous bone.

Figure 6f shows the elongation properties of fabricated polymer nanocomposites. The elongation percentage of polymer composites was reduced due to the functionalized ceramic particulate reinforcement with the PEEK matrix. The addition of T-NPs with PEEK reveals that the increased percentage of elongation. The minimum elongation was observed as 1.39% at 12 wt.%, and the maximum elongation percentage was observed as 2.21% at 8 wt.% T-NPs reinforcement. The addition of S-NPs with PEEK increased elongation percentage up to 12 wt.% of reinforcement, which then tended to decrease. The minimum and maximum elongation percentage observed due to the addition of S-NPs into the PEEK matrix was 1.37% and 1.55%. The combined effect of TS-NPs addition into the PEEK matrix reveals that the maximum and minimum elongation percentage is from 2.01% to 1.41%. From this investigation, the tensile elongation decreases with increases in reinforcement content. Compared to the selected group of composites, the TS/PEEK group was found to have higher tensile properties compared to other groups, and minimum tensile effects were revealed from the S/PEEK group compared to other groups.

## Flexural properties of TS/PEEK composites

The flexural properties of different wt.% of T-NPs and S-NPs reinforced PEEK polymer nanocomposites were investigated according to ASTM-D790. The flexural strength of pure PEEK was shown in Fig. 5b and the obtained experimental stress–strain plots were shown in Fig. 7a-c. The flexural strength and modulus of pure PEEK were 148.727 MPa and 12.86 GPa, respectively. Figure 7d shows increases in T-NPs wt.% with PEEK showed increases in flexural strength. Initially, the flexural strength increases with addition of T-NPs,

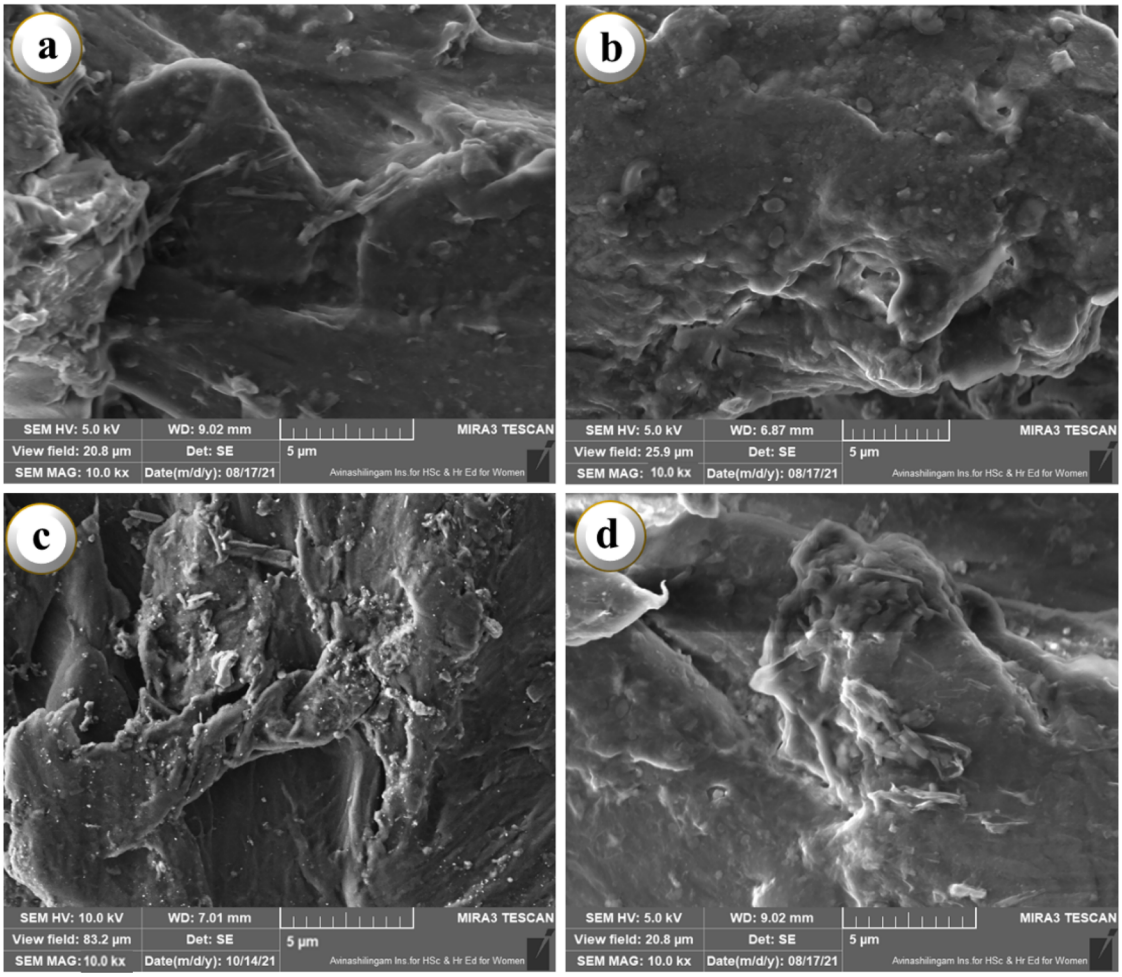


**Fig. 4** FESEM morphologies (**a**-**d**) and EDAS spectra (**e**–**h**) of neat PEEK sample, T/PEEK, S/PEEK and TS/PEEK group composites

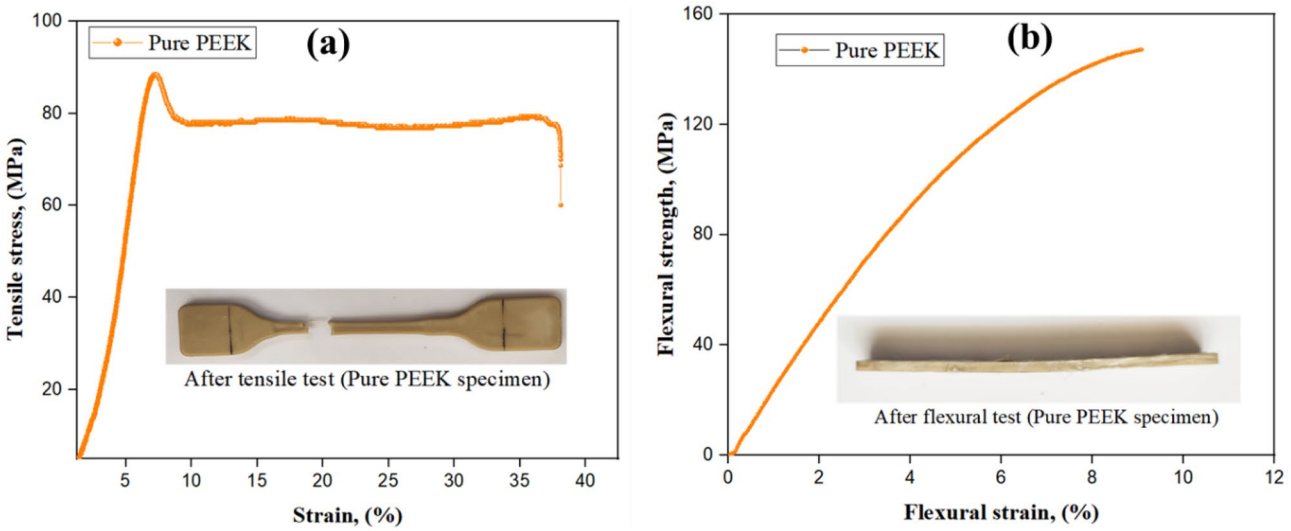


**Fig. 5** **a** Tensile and **b** flexural test stress strain plots for pure PEEK

ranges from 174.65 to 325.25 MPa. The flexural strength increases with the increase of S-NPs wt.% in the PEEK matrix. The range of flexural strength was observed due to the addition of S-NPs was 156.47 MPa to 258.35 MPa. A similar trend was observed while adding the TS-NPs with PEEK that was the flexural strength increases with increases of reinforcement content. The minimum and maximum flexural strength was monitored due to the addition of TS-NPs were about 170.96 MPa and 340 MPa, respectively. The experimental flexural modulus of TS-NPs/PEEK composites is shown in Fig. 7e. the addition of T-NPs content into PEEK provided initially decreased flexural modulus up to 8 wt.%, and then it tends to increase the flexural modulus. The effect of S-NPs and the combined effect of TS-NPs gives the increased flexural modulus. The maximum flexural modulus obtained in T/PEEK, S/PEEK, and TS/PEEK were 38.15 GPa, 37.97 GPa, and 37.32GPa, respectively.

## Compressive properties of TS/PEEK composites

The compressive properties of T-NPs and S-NPs reinforced polymer nanocomposites were investigated as per the ASTM-D695 standard were shown in Fig. 8. The compressive strength and compressive modulus of PEEK were observed as 57.97 MPa and 3.36 GPa, respectively. The addition of T-NPs into PEEK increases the compressive strength and modulus up to 16 wt.%, and then it begins to decrease. The maximum compressive strength and modulus were observed as 67.14 MPa and 4.28 GPa, respectively, at the T/PEEK group. The maximum compressive strength and modulus were obtained due to the addition of S-NPs with PEEK as 65.52 MPa and 3.97 GPa, respectively. The limited improvement of the strength and modulus in the S/PEEK composite group might be attributed to the agglomeration of S-NPs with the PEEK matrix. The combined effect of TS-NPs on PEEK towards compressive strength and modulus was investigated. The range of compressive strength and modulus was obtained due to the addition of TS-NPs was about 42.68 MPa – 71.65 MPa and 3.46 GPa – 4.79 GPa, respectively. The maximum compressive properties were identified at 16 wt.% addition to PEEK. This improvement was due to the synergetic effect between T-NPs and S-NPs.

Implant materials must be able to withstand mechanical stress in order to be effective. To facilitate cell adhesion and proliferation, it is thought that the mechanical characteristics of medical implants should mirror those of the surrounding connective bone tissue. There is a range of compressive strength and modulus for human cancellous bone and cortical bone in the range of 0.1–16 MPa for cancellous bone and 130–180 MPa for cortical bone, respectively [38, 39]. A good compressive strength was found in the 16 wt.% T/PEEK, 12 wt.% S/PEEK, and 16 wt.% TS/PEEK composites in this study. It was clearly shown that all of these values were significantly closer than those of cancellous bone and near to the values of cortical bone. These properties were selected for further FEM analysis to predict the stresses at bone-implant interactions.

## Shore D hardness

The effect of different wt.% of reinforcement with PEEK on shore D hardness are investigated and depicted in Fig. 9. The Shore D hardness of injection moulded virgin PEEK was noted about 82.3. The reinforcement of T-NPs led increase in the shore D hardness of composite samples. The inclusion of T-NPs showed increases in hardness value up to 16

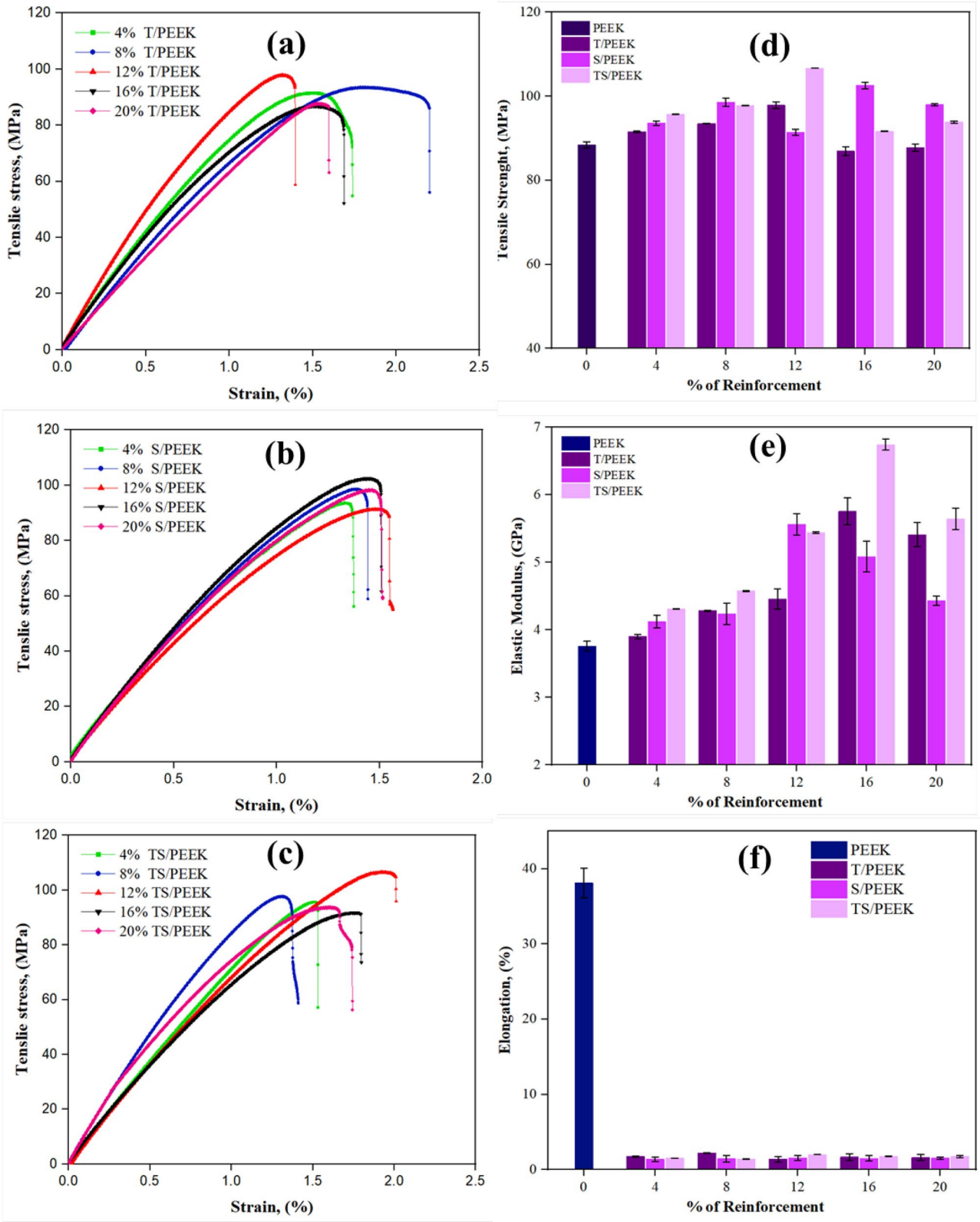


**Fig. 6** Stress–strain plots (**a**-**c**) and tensile properties (**d**-**f**) of neat PEEK sample, T/PEEK, S/PEEK, and TS/PEEK group composites

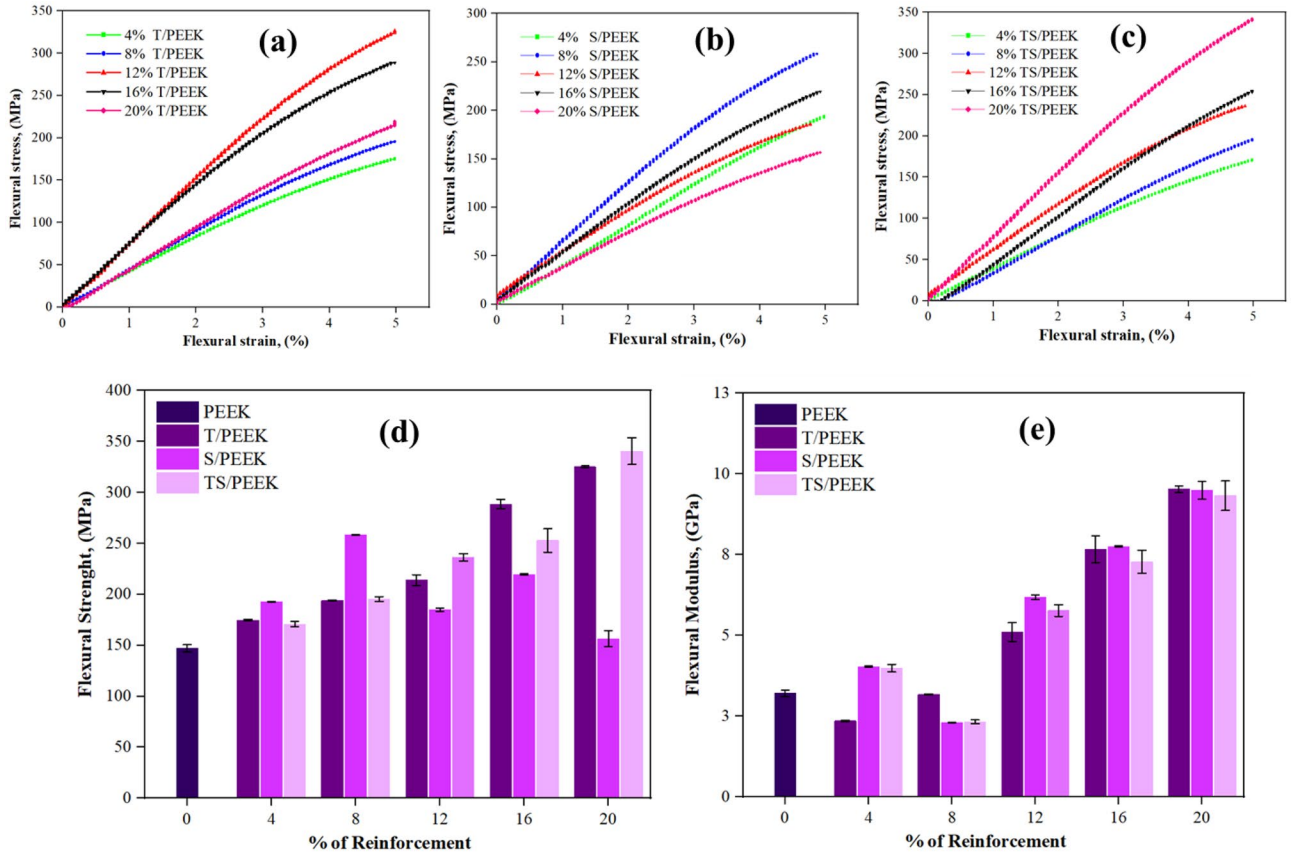


**Fig. 7** Stress–strain plots (**a**-**c**) and flexural properties (**d**, **e**) of T/PEEK, S/PEEK, and TS/PEEK composites with different wt.% of reinforcements

wt.%, and the maximum percentage addition has given the maximum hardness value as 90.1 at 16 wt.%. Then the hardness value get decreases to 89.9. The composite sample was able to withstand local plastic deformation because of the reduced inter-particle distance and increased reinforced filler loading [40]. While adding the S-NPs. The hardness value

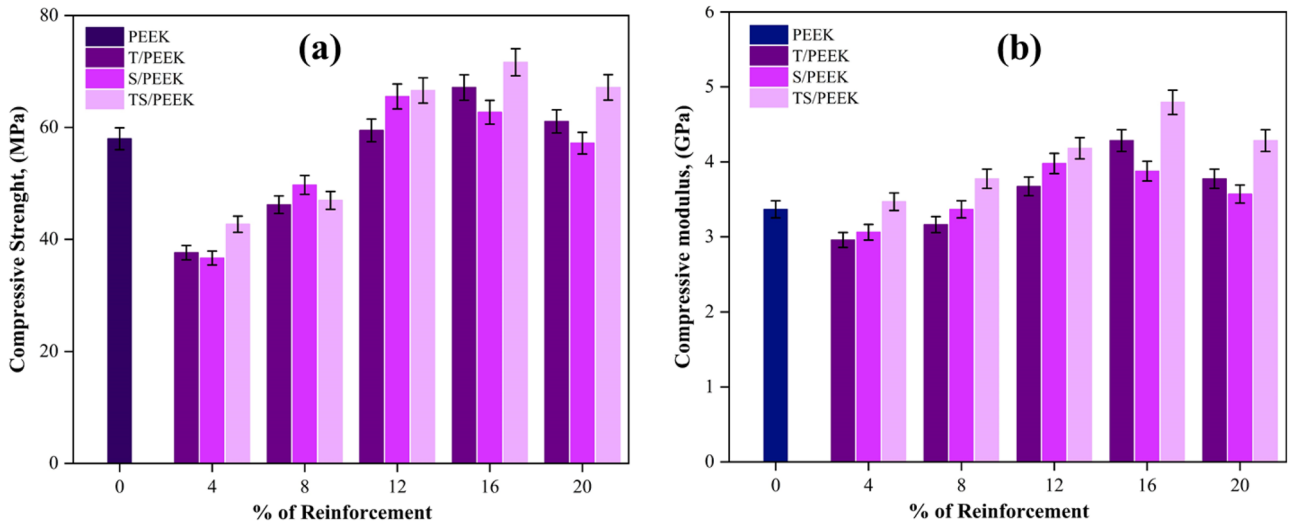


**Fig. 8** Compressive properties (**a** and **b**) of T/PEEK, S/PEEK and TS/PEEK composites with different wt.% of reinforcements

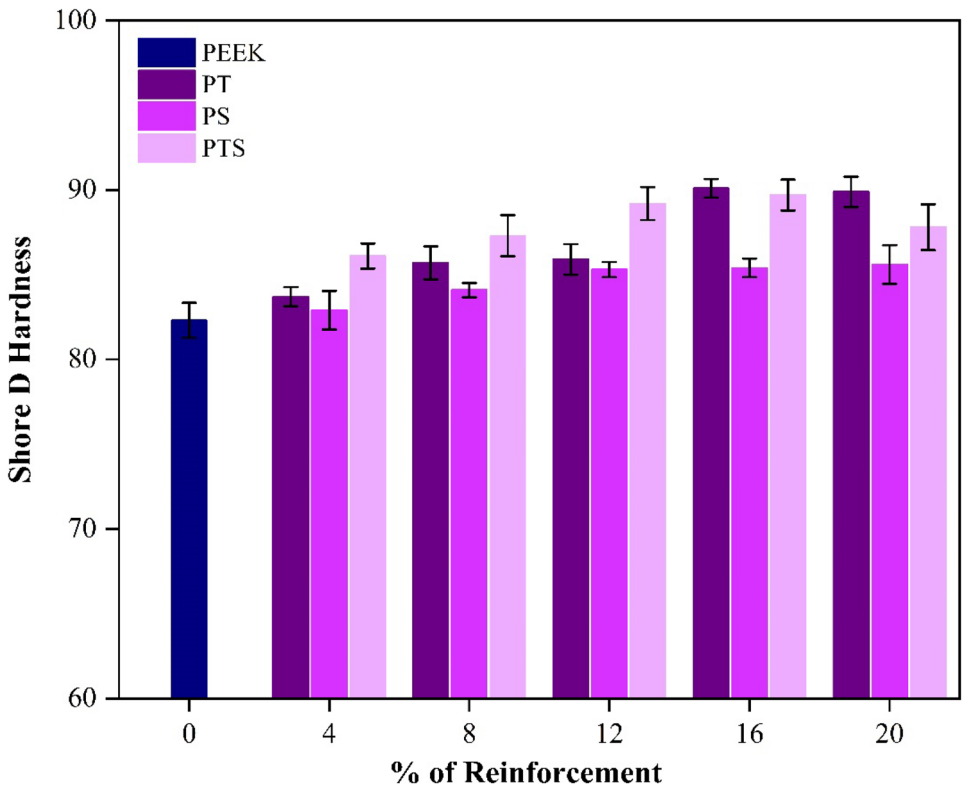


**Fig. 9** Shore D Hardness of T/PEEK, S/PEEK and TS/PEEK composites

increased up to 85.6 at 12 wt.% and then started to decrease. Nanoparticle agglomeration and lower matrix interaction are two possible reasons for this phenomenon [41]. The combined effect of TS-NPs on PEEK towards hardness exhibited good hardness properties. The minimum and maximum shore D hardness values were recorded as 86.1 and 92.4. A larger bonding capacity means that the functionalized NPs have more toughness and strength. They had a greater impact on the hardness of the PEEK matrix and functionalized NPs because of their larger aspect ratio. This has a noticeable impact on the transfer of load [42]. The hardness value was also raised as a result of the increased NP content. The functionalized NPs interfacial adherence to the PEEK matrix is the primary reason for their detachment and improved integration. There was a noticeable difference in shore D hardness between T/PEEK and TS/PEEK, as seen in Fig. 8 when compared to T/PEEK or S/PEEK.

## In-vitro antibacterial assessment

PEEK and selected wt.% polymer composite samples (16 wt.% T/PEEK, 12 wt.% S/PEEK, and 16 wt.% TS/PEEK) were tested for their antibacterial properties against *E. coli* and *B. subtilis* using the disc diffusion method. It has been determined that these two prokaryotic bacterial strains have been introduced to the wound. PEEK and composite samples inhibited *E. coli* and *B. subtilis* growth in the dark condition, as shown in Fig. 10a, b. When tested against *E. coli* and *B. subtilis*, the inhibition zone diameter for PEEK was measured as 9.213 mm and 10.452 mm. And compared to the inhibition zone diameter for polymer composites which is depicted in Fig. 10c. In comparison to pure PEEK polymer, the addition of functionalized T-NPs and S-NPs has shown a considerable improvement in antibacterial activity. The mean diameter of the inhibition zone of 16 wt.% T/PEEK, 12 wt.% S/PEEK and 16 wt.% TS/PEEK composite were monitored as 10.5, 11.9, and 18.299 mm respectively against *E. coli* and 12.25, 13.65, and 16.125 mm against *B. subtilis*, respectively. It revealed that the mean inhibition zone diameter of 16 wt.% T/PEEK, 12 wt.% S/PEEK and 16 wt.% TS/PEEK composite was improved than pure PEEK. Thus, it was confirmed that the absence of UV irradiation also has a favorable antibacterial impact on T-NPs and S-NPs reinforced polymer composites.

T-NPs and S-NPs were found to have similar antibacterial effects on the strains under UV and dark conditions in prior studies [30]. In dark conditions, T-NPs in the rutile phase showed significant antibacterial activity. Exogenous ROS production in a dark environment (lack of UV irradiation) can be explained and confirmed by previous antibacterial research outcomes [43, 44].The above-mentioned data strongly confirms that the increased antibacterial activity of the polymer composite formed from the zone of inhibition. Polymer composites selected for dental implant applications

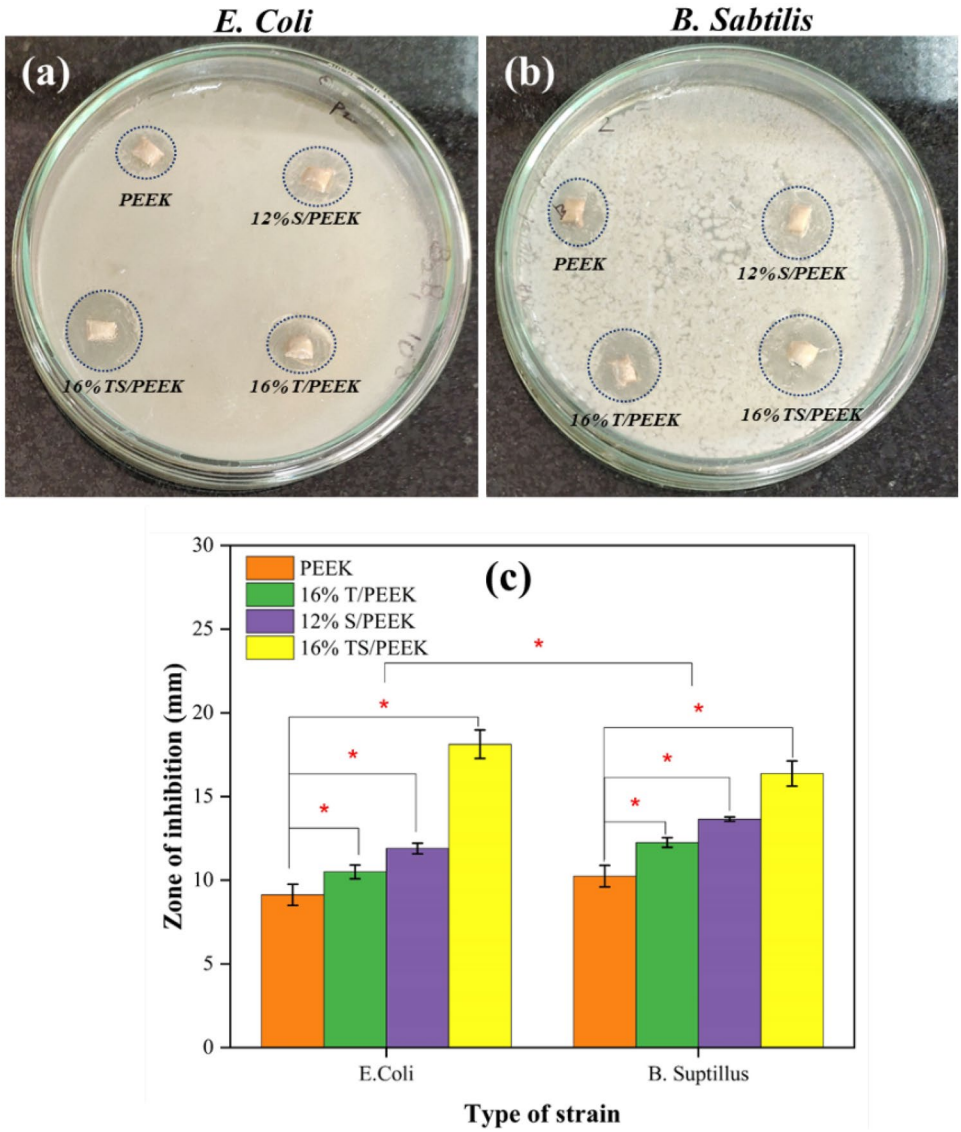


**Fig. 10** Photographs of antibacterial activity results of PEEK, 16% T/PEEK, 12% S/PEEK, AND 16% TS/PEEK nanocomposite (**a** and **b**) against *E. coli* and *B. subtilis*. **c** Zone of inhibitions. (n = 4, * indicates the $p < 0.05$)

have strong antibacterial properties, making them a more viable material.

## Bone stress prediction using 3D FEM

Different colored contours showed the distribution of stress patterns. The von-misses equivalent stress (VMES) at the interface junction of cortical/cancellous bone and implant body under inclined buccolingual load conditions of 60 N was shown in Figs. 11, 12, and 13. The maximum and minimum VMES were tabulated in Table 3 for various thread profiles. These stresses were evaluated by buccolingual load condition with selected composite groups of implants having various profile shapes. The scale in the color bar indicates red and blue with a range of differences. Blue indicates the lowest stress region, and red indicates the higher-stress region. The minimum VMES predicted at cortical bone due to the trapezium profile thread with 16 wt.% TS/PEEK category implants at 60 N load is 0.11 MPa, and maximum stress of 12.14 MPa was found due to the 16 wt.% T/PEEK group implant. The maximum stress region found at cancellous bone due to a buccolingual load of 60 N is 2.45 MPa in buttress threaded implant. At trapezium thread fixation on the cancellous bone region, the minimum stress was noticed at about 0.02 MPa. Due to the buccolingual load of 60 N, maximum stress was found at the cortical bone region in the square threaded implant. Comparatively, 16 wt.% TS/PEEK category implants have a minimum stress distribution in cortical and cancellous bone than 16 wt.% T/PEEK and 14 wt.% S/PEEK. The 16 wt.% T/PEEK category implants having maximum stress distribution at the bone interface. The stress distribution is minimum while using TS/PEEK with trapezium profile threaded implant.

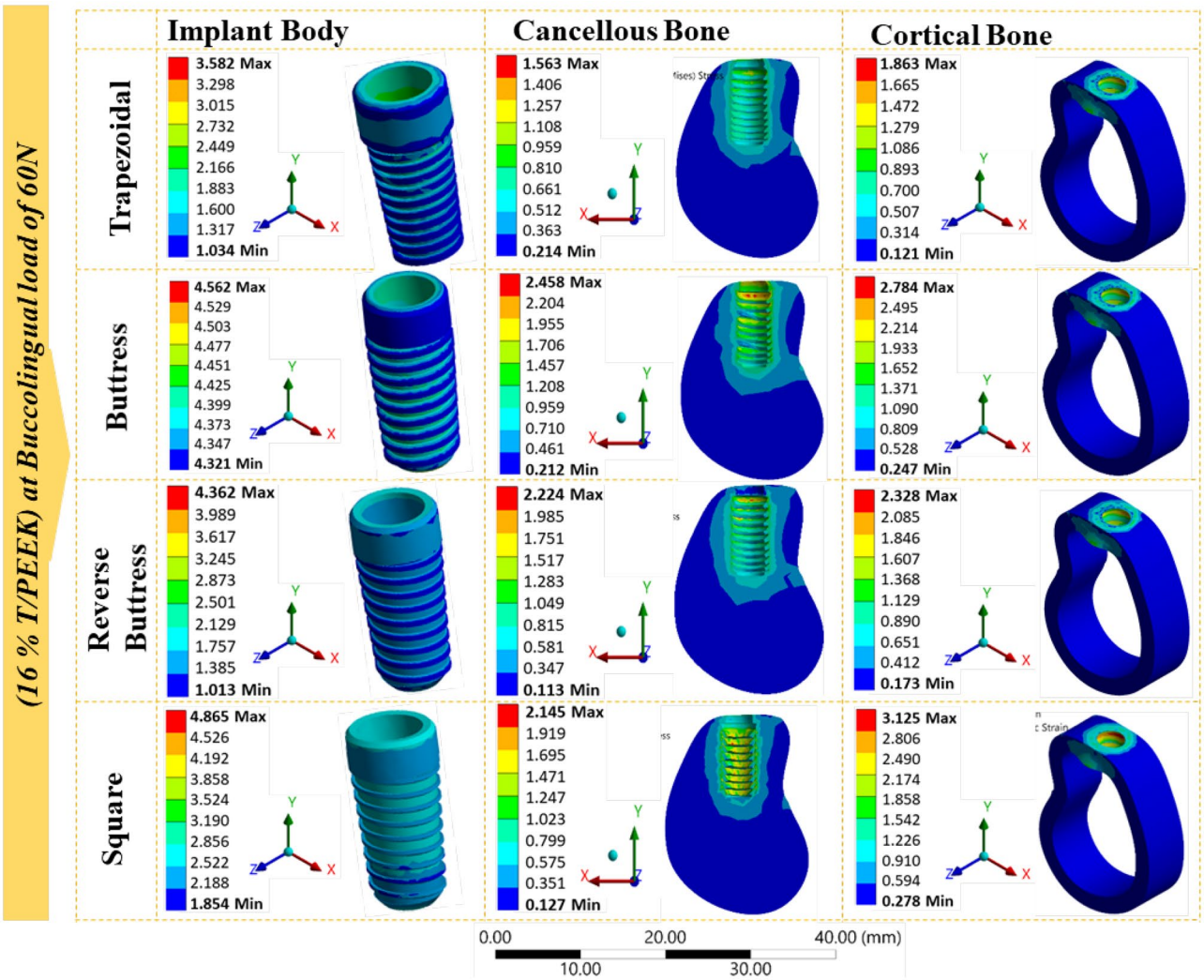


**Fig. 11** Stress distribution (MPa) contours for 16 wt.% T/PEEK implant body, cancellous and cortical bone with different types of thread profile due to buccolingual load of 60 N

Implant thread profile plays a significant role in deciding the value of initial Bone-Implant Contact (BIC) regions with respect to the density of bone at 60 N loading conditions. The square threaded implants are showing less Functional Surface Area (FSA), which means minimum initial contact [45]. Trapezium threaded implants have a maximum initial contact design to improve the FSA, which dissipates the load to the bone-implant interface. Buttress and reverse buttress type profiles are also designed to maximize the FSA in order to distribute the load to all interface regions of bone/implant. But comparing the stress values after analysis, the buttress and reverse buttress design have comparatively maximum stress values because of minimum FSA compared to trapezium thread, and it was found as the highest stress distribution [46]. Trapezium implant design has maximum initial contact to improve the FSA and distribute the applied axial and buccolingual load to the interface to achieve minimum stress.

The primary objective of functional design implemented in dental implants is to dissipate and distribute the biomechanical forces to the interface region of bone/implant [47]. Occlusal loads in poor density bone regions want to compensate by providing an excellent and optimized implant design. The smooth neck portion of the implant design provides the highest initial contact area with the cortical bone [48]. So that distribution of load or load transmitting marginally even. Because of this condition, the development of stress at the cortical bone interface becomes minimum, which confirms that the design is safer. Bone and implants are highly complicated structures for that, FEM is utilized as a reliable tool to predict the development of stresses in various components that is not possible by in-vivo studies.

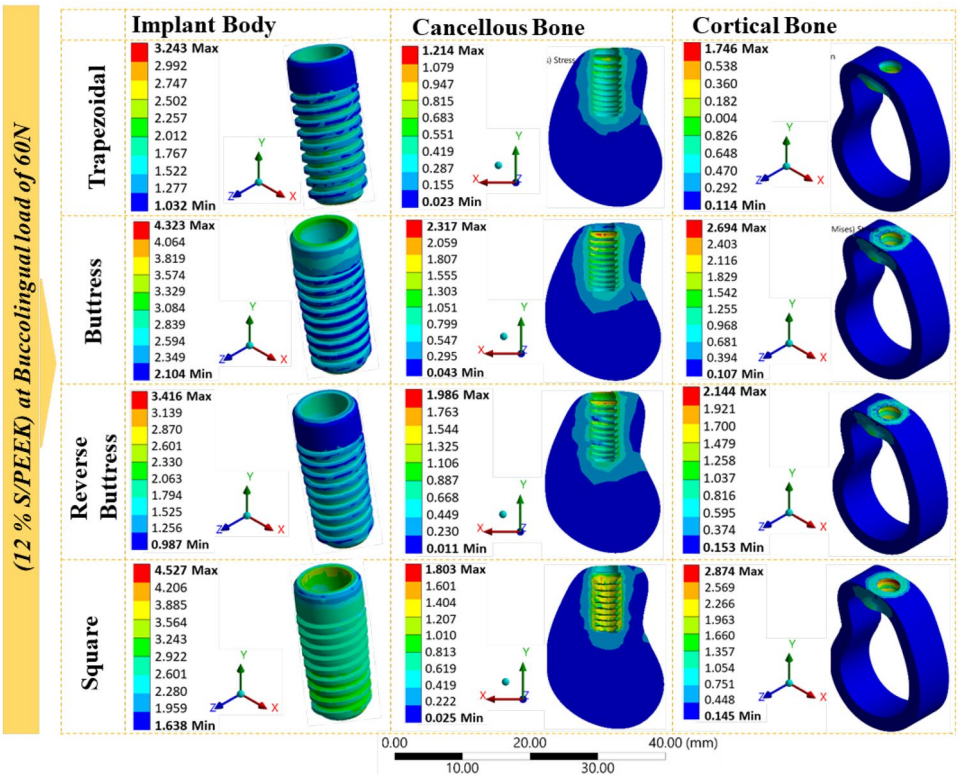


**Fig. 12** Stress distribution (MPa) contours for 12 wt.% S/PEEK implant body, cancellous and cortical bone with different types of thread profile due to buccolingual load of 60 N

FEM-related studies generally deal with directions of stress types (shear, compression, and tension) or the magnitude of principal stresses (VMES). The VMES is an effective way of the exact magnitude of stress taken into account in the 3D analysis of stress. Some limitations are also there while performing for predicting stresses FEA not given the

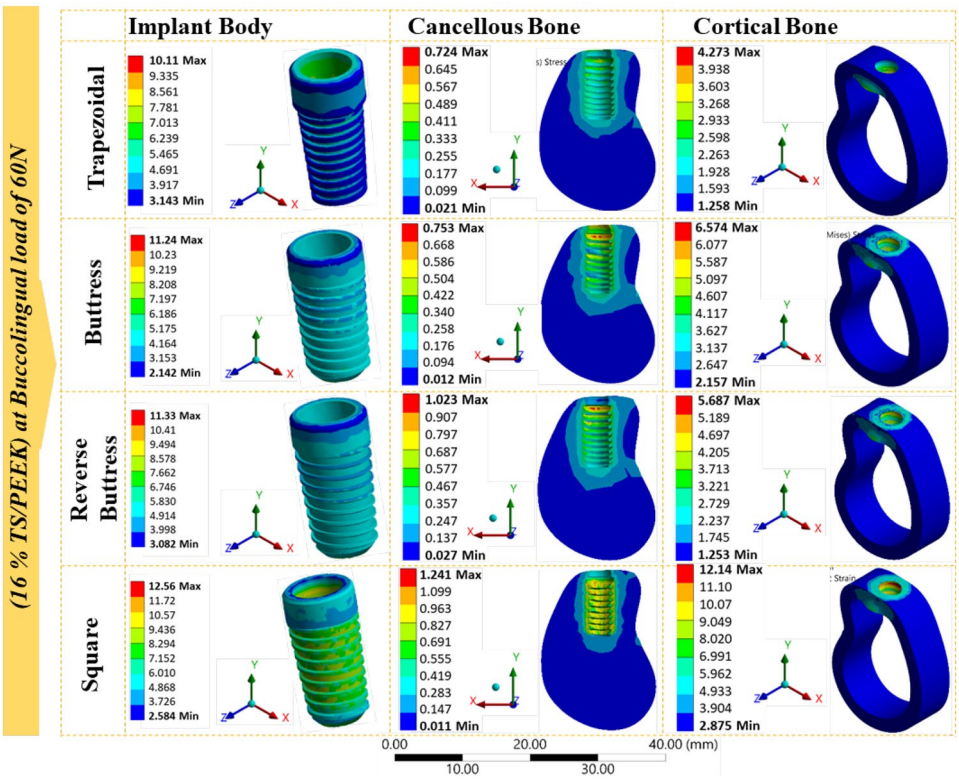


**Fig. 13** Stress distribution (MPa) contours for 16 wt.% TS/PEEK implant body, cancellous and cortical bone with different types of thread profile due to buccolingual load of 60 N

**Table 3** Von-Misses stresses (MPa) at bone and implant body due to the buccolingual load of 60 N

| Von-Misses stress at a buccolingual load of 60 N | | Thread profile shape | | | | | | | |
|---|---|---|---|---|---|---|---|---|---|
| | | Trapezium | | Buttress | | Reverse Buttress | | Square | |
| | | Min (MPa) | Max (MPa) | Min (MPa) | Max (MPa) | Min (MPa) | Max (MPa) | Min (MPa) | Max (MPa) |
| **Implant body** | **16% T/PEEK** | 3.14 | 10.11 | 2.14 | 11.24 | 3.08 | 11.33 | 2.58 | 12.56 |
| | **12% S/PEEK** | 1.24 | 3.58 | 1.25 | 4.56 | 1.01 | 4.36 | 1.85 | 4.86 |
| | **16% TS/PEEK** | 1.03 | 3.24 | 2.1 | 4.32 | 0.98 | 3.41 | 1.63 | 4.52 |
| **Cancellous bone** | **16% T/PEEK** | 0.02 | 0.72 | 0.01 | 0.75 | 0.02 | 1.02 | 0.01 | 1.24 |
| | **12% S/PEEK** | 0.21 | 1.56 | 0.21 | 2.45 | 0.11 | 2.22 | 0.12 | 2.14 |
| | **16% TS/PEEK** | 0.02 | 1.21 | 0.04 | 2.31 | 0.01 | 1.98 | 0.02 | 1.8 |
| **Cortical bone** | **16% T/PEEK** | 1.25 | 4.21 | 2.15 | 6.57 | 1.25 | 5.68 | 2.87 | 12.14 |
| | **12% S/PEEK** | 0.12 | 1.86 | 0.24 | 2.78 | 0.17 | 2.32 | 0.27 | 3.12 |
| | **16% TS/PEEK** | 0.11 | 1.74 | 0.1 | 2.69 | 0.15 | 2.14 | 0.14 | 2.87 |

exact value from in-vivo or in-vitro studies. This study may have some deviations: bone material is linearly elastic and homogenous. Still, natural bone is visco-elastic, heterogeneous, and isotropic material. The resultant stress values are accepted quantitatively, not quantitatively, due to the application of static loading. Whereas naturally, they are dynamic while chewing. Due to the limitations of this study, further clinical evaluation is required the further future work in the form of in-vitro and in-vivo studies.

## Conclusion

In this study, the T-NPs and S-NPs were utilized as reinforcements and developed T/PEEK, S/PEEK, and TS/PEEK polymer nanocomposites using vertical plastic injection moulding machine with different wt.% such as 4, 8, 12, 16, and 20 wt.%. The proper distribution and dispersion of NPs with the PEEK matrix were observed by FE-SEM morphological analysis. The mechanical characterization of developed polymer composite groups has been evaluated through tensile, flexural, compressive, and Shore D hardness testing. The maximum tensile strength was measured as 106.747 MPa at 12 wt.% of TS/PEEK compared to other groups, and maximum elastic modulus was observed as 6.64 GPa at 16 wt.% of the TS/PEEK group. The maximum flexural strength was observed as 267.06 MPa at 20 wt.% TS/PEEK group. After comparing T/PEEK and S/PEEK groups, the maximum compressive strength and compressive modulus were obtained as 71.65 MPa and 4.79 GPa, respectively, at 16 wt.% TS/PEEK group. The highest shore D hardness value was obtained as 92.4 at 16 wt.% TS/PEEK group followed by T/PEEK and S/PEEK. Based on maximum compressive properties and hardness values, the best combinations were selected, such as 16 wt.% T/PEEK, 12 wt.% S/PEEK, and 16 wt.% TS/PEEK in all three groups. Further, the in-vitro antibacterial activity of selected polymer composites was assessed and found that the excellent antibacterial property against *E. coli* and *B. subtilis.* The maximum zone of inhibition was monitored at 16 wt.% TS/PEEK sample compared to T/PEEK and S/PEEK. The cortical and cancellous bone stresses were predicted in implant models with four different thread profiles at osteointegration. The minimum stress distribution around the implant at the human cortical and cancellous bone model was predicted as 0.11–1.74 MPa while using trapezium profile threaded implants. Hence, it was confirmed that the developed composites could be a suitable candidate for medical implant applications and further in-vivo studies.

**Funding** The author(s) have no funding from any agencies to report.

## Declarations

**Conflict of interest** There are no potential conflicts of interest was reported between the author(s).

## References

1. Kuo MC, Tsai CM, Huang JC, Chen M (2005) PEEK composites reinforced by nano-sized SiO2 and A12O3 particulates. Mater Chem Phys 90(1):185–195
2. Chen SG, Yang J, Jia YG, Lu B, Ren L (2019) TiO2 and PEEK reinforced 3d printing pmma composite resin for dental denture base applications. Nanomaterials 9(7):1049
3. Gong Y, Tian W, Zhang P, Chen J, Zhang Y, Sun Z (2019) Slip casting and pressureless sintering of Ti3AlC2. J Adv Ceram 8(3):367–376
4. Alamgir M, Nayak GC, Mallick A, Sahoo S (2021) Effects of TiO2 and GO nanoparticles on the thermomechanical

properties of bioactive poly-HEMA nanocomposites. Iran Polym J 30(10):1089–1099
5. Tu-Morn M, Pairoh N, Sutapun W, Trongsatitkul T (2019) Effects of titanium dioxide nanoparticle on enhancing degradation of polylactic acid/low density polyethylene blend films. Mater Today Proc 17:2048–2061
6. Tangudom P, Martín-Fabiani I, Prapagdee B, Wimolmala E, Markpin T, Sombatsompop N (2021) Improvement of mechanical-antibacterial performances of AR/PMMA with TiO2 and HPQM treated by N-2(aminoethyl)-3-aminopropyl trimethoxysilane. J Reinf Plast Compos 40(13):477–489
7. Mourad AHI, Mozumder MS, Mairpady A, Pervez H, Kannuri UM (2017) On the injection molding processing parameters of HDPE-TiO2 nanocomposites. Materials (Basel) 10(1):1–25
8. Shi G, Cao Z, Yan X, Wang Q (2019) In-situ fabrication of a UHMWPE nanocomposite reinforced by SiO2 nanospheres and its tribological performance. Mater Chem Phys 26:121778
9. Zuo Y, Chen K, Li P, He X, Li W, Wu Y (2020) Effect of nano-SiO2 on the compatibility interface and properties of polylactic acid-grafted-bamboo fiber/polylactic acid composite. Int J Biol Macromol 157:177–186
10. Yu M, Huang J, Zhu T, Lu J, Liu J, Li X, Yan X, Liu F (2020) Liraglutide-loaded PLGA/gelatin electrospun nanofibrous mats promote angiogenesis to accelerate diabetic wound healing: Via the modulation of miR-29b-3p. Biomater Sci 8(15):4225–4238
11. Lu Z, Wang W, Zhang J, Bártolo P, Gong H, Li J (2020) Electrospun highly porous poly(L-lactic acid)-dopamine-SiO2 fibrous membrane for bone regeneration. Mater Sci Eng C 117:111359
12. Wu X, Liu X, Wei J, Ma J, Deng F, Wei S (2012) Nano-TiO2/PEEK bioactive composite as a bone substitute material: In vitro and in vivo studies. Int J Nanomedicine 7:1215–1225
13. Aumnakmanee S, Yodpiji N, Jantong N, Jongprasithporn M (2018) Finite element analysis of dental implant prosthetics. Mater Today Proc 5(3):9525–9534
14. Dhatrak P, Shirsat U, Sumanth S, Deshmukh V (2018) Finite Element Analysis and Experimental Investigations on Stress Distribution of Dental Implants around Implant-Bone Interface. Mater Today Proc 5(2):5641–5648
15. Pirmoradian M, Naeeni HA, Firouzbakht M, Toghraie D, khabaz MK, Darabi R (2020) Finite element analysis and experimental evaluation on stress distribution and sensitivity of dental implants to assess optimum length and thread pitch. Comput Methods Programs Biomed 187
16. Ryu HS, Namgung C, Lee JH, Lim YJ (2014) The influence of thread geometry on implant osseointegration under immediate loading: A literature review. J Adv Prosthodont 6(6):547–554
17. Niroomand MR, Arabbeiki M (2020) Implant stability in different implantation stages: Analysis of various interface conditions. Informatics Med 19:100317
18. Xian P, Chen Y, Gao S, Qian J, Zhang W, Udduttula A, Huang N, Wan G (2020) Polydopamine (PDA) mediated nanogranular-structured titanium dioxide (TiO2) coating on polyetheretherketone (PEEK) for oral and maxillofacial implants application. Surf Coatings Technol 401:126282
19. Sharma C, Kalra T, Kumar M, Bansal A, Chawla AK (2020) To Evaluate the Influence of Different Implant Thread Designs on Stress Distribution of Osseointegrated Implant: A Three-Dimensional Finite-Element Analysis Study–An In Vitro Study. Dent J Adv Stud 8(1):9–16
20. Gupta S (2016) Dental Implants and Dentures : Open Access A Recent Updates on Zirconia Implants : A Literature Review 1(1):1–6
21. Thanigachalam M, Muthusamy Subramanian AV (2022) In-vitro cytotoxicity assessment and cell adhesion study of functionalized nTiO2 reinforced PEEK biocompatible polymer composite. Polymer-Plastics Technology and Materials 61(5):566–576
22. Thanigachalam M, Muthusamy Subramanian AV (2022) Evaluation of PEEK-TiO2-SiO2 nanocomposite as biomedical implants with regard to in-vitro biocompatibility and material characterization. J Biomater Sci Polym Ed 33(6):727–746
23. Harting R, Barth M, Bührke T, Pfefferle RS, Petersen S (2017) Functionalization of polyetheretherketone for application in dentistry and orthopedics. Bio Nano Materials 18(1–2)
24. Ghomi ER, Khorasani SN, Kichi MK, Dinari M, Ataei S, Enayati MH, Koochaki MS, Neisiany RE (2020) Synthesis and characterization of TiO2/acrylic acid-co-2-acrylamido-2-methyl propane sulfonic acid nanogel composite and investigation its self-healing performance in the epoxy coatings. Colloid Polym Sci 298(2):213–223
25. Balaji Ayyanar C, Marimuthu K (2020) Investigation on the morphology, thermal properties, and in vitro cytotoxicity of the fish scale particulates filled high-density polyethylene composite. Polym Polym Compos 28(4):285–296
26. Suresh V, Hariharan N, Paramesh S, Prasath Kumar M, Arun Prasath P (2016) Tribological behaviour of aluminium/boron carbide (B4C)/graphite (Gr) hybrid metal matrix composite under dry sliding motion by using ANOVA. Int J Mater Prod Technol 53(3–4):204–217
27. Schwitalla AD, Spintig T, Kallage I, Müller WD (2015) Flexural behavior of PEEK materials for dental application. Dent Mater 31(11):1377–1384
28. Kolken HMA, Lietaert K, van der Sloten T, Pouran B, Meynen A, Van Loock G, Weinans H, Scheys L, Zadpoor AA (2020) Mechanical performance of auxetic meta-biomaterials. J Mech Behav Biomed Mater 104:103658
29. Xu A, Liu X, Gao X, Deng F, Deng Y, Wei S (2015) Enhancement of osteogenesis on micro/nano-topographical carbon fiber-reinforced polyetheretherketone-nanohydroxyapatite biocomposite. Mater Sci Eng 48:592–598
30. Bokare A, Sanap A, Pai M, Sabharwal S, Athawale AA (2018) Antibacterial activities of Nd doped and Ag coated TiO2 nanoparticles under solar light irradiation. Colloids Surfaces B Biointerfaces 102:273–280
31. Shehzad A, Qureshi M, Jabeen S, Ahmad R, Alabdalall AH, Aljafary MA, Al-Suhaimi E (2018) Synthesis, characterization and antibacterial activity of silver nanoparticles using Rhazya stricta. PeerJ 12:1–15
32. Chen S, Yang J, Li K, Lu B, Ren L (2018) Carboxylic acid-functionalized tio2 nanoparticle-loaded pmma/ peek copolymer matrix as a dental resin for 3d complete denture manufacturing by stereolitographic technique. Int J Food Prop 21(1):2557–2565
33. Jaganathan SK, Prasath Mani M, Ayyar M, Rathanasamy R (2019) Biomimetic electrospun polyurethane matrix composites with tailor made properties for bone tissue engineering scaffolds. Polym Test 78:1
34. Aruna STR, Shilpa M, Lakshmi RV, Balaji N, Kavitha V, Gnanamani A (2018) Plasma Sprayed Hydroxyapatite Bioceramic Coatings from Coprecipitation Synthesized Powder: Preparation, Characterization and in vitro Studies. Trans Indian Ceram Soc 77(2):90–99
35. Ramesh M, Sudharsan P (2018) Experimental Investigation of Mechanical and Morphological Properties of Flax-Glass Fiber Reinforced Hybrid Composite using Finite Element Analysis. SILICON 10(3):747–757
36. Gonçalves J, Lima P, Krause B, Pötschke P, Lafont U, Gomes JR, Abreu CS, Paiva MC, Covas JA (2018) Electrically conductive polyetheretherketone nanocomposite filaments: From production to fused deposition modeling. Polymers 10(8):1–20
37. Ahamad A, Kumar P (2021) Mechanical and thermal performance of PEEK/PEI blend matrix reinforced with surface modified halloysite nanotubes. J Thermoplast Compos Mater. https://doi.org/10.1177/08927057211028629

38. Tzibula S, Lovinger Z, Rittel D (2018) Dynamic tension of ductile polymers: Experimentation and modelling. Mech Mater 123:30–42
39. Ravichandran M, Veerappan G, Dhinakaran V, Katiyar JK (2021) Optimization of tribo-mechanical properties of boron carbide reinforced magnesium metal matrix composite. Proc Inst Mech Eng Part J J Eng Tribol 1–13
40. Yoon JI, Kim JG, Jung JM, Jeong HJ, Lee S, Kim HS, Lee DJ, Shahbaz M (2016) Obtaining reliable true plastic stress-strain curves in a wide range of strains using digital image correlation in tensile testing. J Korean Inst Met Mater 54(4):231–236
41. Keyvani A, Mostafavi N, Bahamirian M, Sina H, Rabiezadeh A (2020) Synthesis and phase stability of zirconia-lanthania-ytterbia-yttria nanoparticles; a promising advanced TBC material. J Asian Ceram Soc 8(2):336–344
42. Ayode Otitoju T, Ugochukwu Okoye P, Chen G, Li Y, Onyeka Okoye M, Li S (2020) Advanced ceramic components: Materials, fabrication, and applications. J Ind Eng Chem 85:34–65
43. Díez-Pascual AM, Díez-Vicente AL (2015) Nano-TiO2 reinforced PEEK/PEI blends as biomaterials for load-bearing implant applications. ACS Appl Mater Interfaces 7(9):5561–5573
44. Vargas MA, Rodríguez-Páez JE (2019) Facile Synthesis of TiO 2 Nanoparticles of Different Crystalline Phases and Evaluation of Their Antibacterial Effect Under Dark Conditions Against E. coli. J Clust Sci 30(2):379–391
45. Andreiotelli M, Wenz HJ, Kohal RJ (2009) Are ceramic implants a viable alternative to titanium implants? A systematic literature review. Clin Oral Implants Res 20(4):32–47
46. Almutairi AS, Walid MA, Alkhodary MA (2018) The effect of osseodensification and different thread designs on the dental implant primary stability. F1000Research 7:1–9
47. Hu F et al (2019) Comparison of Three Different Types of Two-Implant-Supported Magnetic Attachments on the Stress Distribution in Edentulous Mandible. Comput. Math. Methods Med. https://doi.org/10.1155/2019/6839517
48. Mao Q, Su K, Zhou Y, Hossaini-Zadeh M, Lewis GS, Du J (2019) Voxel-based micro-finite element analysis of dental implants in a human cadaveric mandible: Tissue modulus assignment and sensitivity analyses. J Mech Behav Biomed Mater 94:229–237